である（図1）．血液中の代謝生成物（$H_2{}^{15}O$）の影響が考慮されていないことによるバイアスと，画質が不十分だという評価がなされている．もうひとつの方法が国立循環器病研究センターから提案されたDual-Autoradiography（DARG）法と呼ばれる方法で，ARG法における$^{15}O_2$と$C^{15}O_2$あるいは$^{15}O_2$と$H_2{}^{15}O$の投与間隔を短縮させたことで，20分間で検査できる（図1）．$C^{15}O$吸入スキャンを行わずCBV画像の計算も行うことで，さらに検査時間を短縮化するDBFM法も提案されている[9]．^{15}Oガス投与はボーラスかあるいは1分間程度であり，CT搭載型のPET装置を利用すれば全体で検査時間は10分間以内にまで短縮できる可能性がある．全血液中の放射能濃度を持続モニターし，かつ動脈血液中の代謝生成物である$H_2{}^{15}O$を数理モデルで補正する手順はARG法と同様である．

定量精度と信頼性

^{15}OガスPET検査では，局所組織酸素消費量などの生理機能を定量的に計測できるといわれながら，真の意味で正当性の確認がなされているわけではなかった．手技上の誤差は報告ごとに異なるため，CBF，$CMRO_2$の正常値ですら報告によって異なる（表1）．対象群の差やガス吸入法などの違いによる真の差もあるが，撮像パラメータや解析手法の違いも少なからず影響を与える．Itohら[10]は国内の11施設における70名の健常者データにおいての施設間差は，手法や設定したパラメータ数値によるものとしている．

Leendersらの報告においても，健常者のCBFや$CMRO_2$が加齢とともに減少するとしながらも，広い範囲に分散している（CBF値が90mL/min/100gから30mL/min/100g，$CMRO_2$値が2.0mL/min/100gから1.3mL/min/100g）のは，手技上の誤差の影響が大である．閉鎖式のフェースマスクが呼吸を不安定なものにし，2時間を超える検査中の変動が，結果として数値の不安定化を来たしていたと考えられている．^{15}Oガス吸入の安定化を図り，開放マスクの利用をもとに行われたYamaguchiらの報告ではCBFが60mL/min/100g～30mL/min/100g程度，$CMRO_2$が4.3mL/min/100g～2.3mL/min/100gに減少した．表1に示すように，概して開放式の吸入法を採用した報告でCBFが低い傾向を認める．呼吸を安定にさせ，侵襲性を軽減する工夫と検査時間の短縮化が^{15}Oガス検査では本質的であると考えられた．

一般にPETで機能画像の定量化を行うには，数理モデルを仮定して画像計算を行う．$^{15}O_2$吸入ガスPET検査では，脳組織に移行した酸素

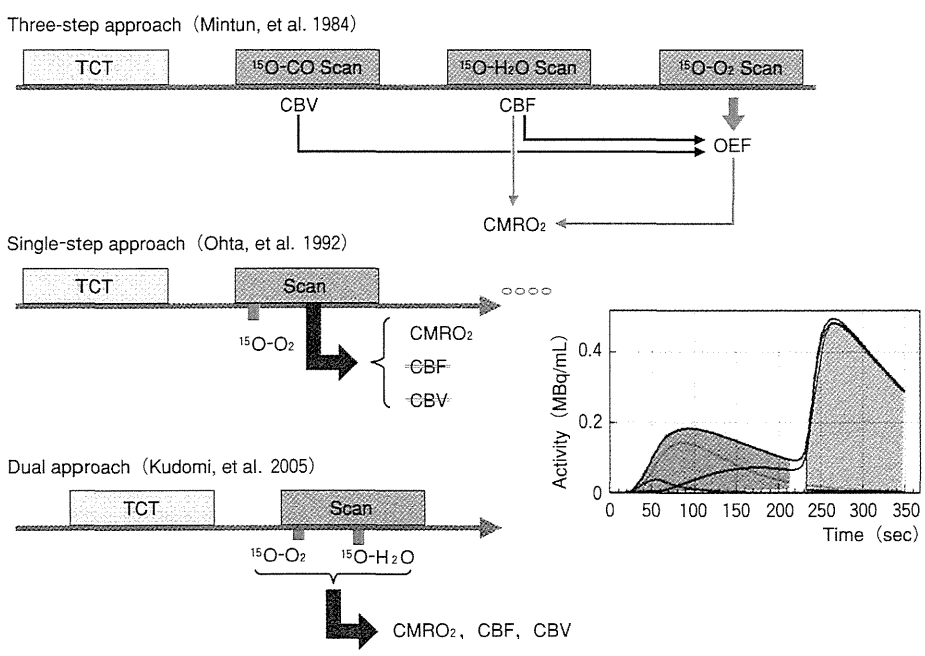

図1 代表的な^{15}OガスPET検査プロトコルの比較

Autoradiographyに代表される3ステップ法では，3つのスキャンごとに異なる放射性薬剤が供給される．1ステップ法では$^{15}O_2$ 1回吸入のみで3つのパラメータを計測することをもくろむが，実際には$CMRO_2$のみが利用される．Dual法では，1回のスキャン中に2種の放射性ガスを吸入する．別に$C^{15}O$吸入スキャンを行うか，あるいは1回のスキャンのみでCBV画像を提示することを試みる．

($^{15}O_2$) は直ちに代謝され $H_2{}^{15}O$ として脳からCBFに従って洗い出される（図2），すなわち酸素としての血液への洗い出しは無視できるほど小さいと仮定している．この仮定は必ずしも実証されたわけではなかったが，近年筆者らの行った検討で，内頸動脈に$^{15}O_2$-標識酸化ヘモグロビンを内頸動脈にボーラス投与した後のクリアランス率が，$H_2{}^{15}O$ をボーラス投与した場合とよく一致することから，本モデルの精度は十分に高いと考える．また，DARG法PET検査をカニクイザル対象に施行したところ，PETで得た脳全体OEF値は内頸静脈の血中酸素分圧から求めたOEF値と，生理的に広い範囲で一致すること（図3）が確認された[11]．迅速化法で初めて示された事実ではあるが，Hattoriらが健常者を対象に確認した報告[12]や，心筋領域におけるOEF定量値の一致に関する報告[13]とあわせて，^{15}O 酸素を用いたPET検査は，きわめて正確に $CMRO_2$ やOEF値を計測し得ることを示す．ただし，種々の手技に依存して結果が変わることについても注意が必要で，たとえばHatazawaらの報告[14]では，他報告と比べてCBF値，$CMRO_2$ 値を約20%高く提示しているが，これは入力関数の遅延（delay）補正における誤差[5]で説明される．このような状況を熟知しておく必要がある．

^{15}O ガスを用いたPET検査で脳循環代謝量を定量評価する場合に，表2に示すような種々の誤差限界がある．PET装置の空間解像度が脳皮質構造と比べると不十分なことに起因する部分容積効果によって，CBFや $CMRO_2$ の定量値を過小評価し，その程度はPET装置固有の空間解像度だけではなく，検査プロトコルや解析法によっても異なる．典型的には50%程度の過小評価もあり

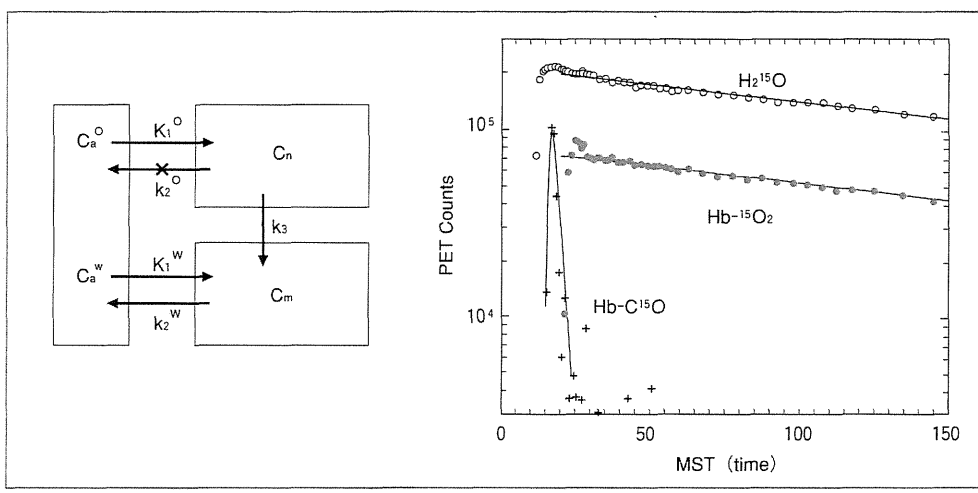

図2 $^{15}O_2$ガスを使った局所脳酸素代謝量（$CMRO_2$）の定量計測の妥当性

脳に移行した$^{15}O_2$は直ちに代謝され $H_2{}^{15}O$ としてCBFにて洗い出されると仮定している．実際に内頸動脈に$^{15}O_2$をボーラス投与した後のクリアランスは，同様に $H_2{}^{15}O$ を投与した場合のクリアランスによく一致する．脳内に酸素分子として残留する分画がきわめて少ないこと，および酸素代謝量計測に利用される動態モデルの妥当性を示唆している．

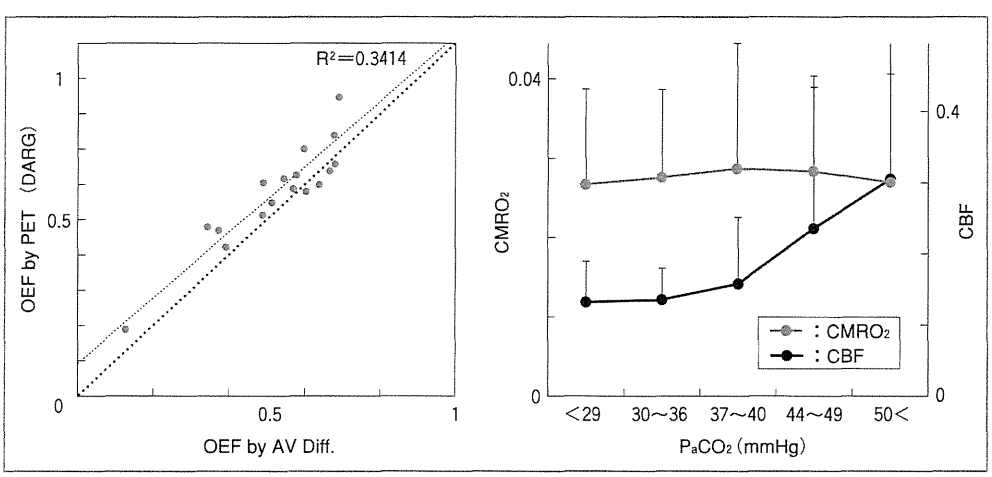

図3 筆者らが行ったカニクイザルを使った妥当性評価の結果

酸素摂取率は内頸静脈採血の酸素分圧から推定した値に，生理的に広い範囲で一致しており，$PaCO_2$ に依存していない．^{15}O ガスを使って酸素消費量や酸素摂取率の絶対定量が可能であることを示す．

（文献11より引用改変）

得るとされる[15,16]が，steady state 法は ARG 法や DARG 法よりも影響が大きい．ARG 法や DARG 法では入力関数の遅延（delay）[5]や，これに基づく形の歪み（dispersion）[6]が誤差要因である．動脈採血時における delay を小さくする工夫や，精度の高い補正，誤差を最小化するようなスキャン時間の選択が本質的である．視野内外に強い放射性ガスが存在することや（図4），短い検査での画像精度の確保は必ずしも容易ではなく，投与量や吸入時間，供給マスクやチューブの影響を排除する工夫も必要である．特に高感度化された3次元 PET（3D PET）装置ではそれらの影響もより多く受け，本質的な精度限界との競争でもある．しかし，^{15}O ガスを吸入するフェースマスクの改良や投与量の最適化，画像再構成理論の改良などにより，十分に高精度で，高解像度かつ高感度の画像を得ることが可能である（図5，6）．空間解像度や画像精度は従来装置と比べて大きく改善した．PET 画像から血中放射能濃度の計測を行うことも可能になり，無採血定量の可能性が広がった．^{15}O ガス PET 検査の新しい応用領域の開拓に貢献するような今後の研究が期待されるところである．種々の検査手順の簡便化と標準化や，被験者に対する負担の軽減や，生理的変動を最小にする工夫も重要である．

技術的課題

^{15}O ガス PET 検査を実際の臨床で実施するには PET 撮像と周辺機器の操作だけでなく，動脈採血と血液データの解析，サイクロトロンの運転，一連の ^{15}O ガスの標識合成，さらに標識合成ごとに QC（安全性試験，純度検定など）などを担当するスタッフの確保が必要である．検査枠の調整は一般には容易ではなく，急性期脳梗塞疾患の検査への対応は困難であった．筆者らは，オンデマンドでも実施し得る ^{15}O ガス PET 検査システムの実用化を目指して技術整備を行ってきた．^{15}O 標識ガス合成装置においては標識合成と品質検定を迅速かつ簡便に実施できるような迅速検査対応型の ^{15}O ガス合成システムの開発に成功し，現在4.5分間隔で異なる ^{15}O 標識ガスを繰り返し供給することが可能になった．すなわち $C^{15}O$ ガス吸入を必要とする DARG 法検査でも全体で20分間程度，$C^{15}O$ ガス吸入を必要としない DBFM 法検査では8～9分間程度で一連の検査を完結させることができる．本 ^{15}O ガス合成・供給装置については，それぞれの放射性ガスを合成，供給終了した後に強制的に排気し，次の標識合成に必要なターゲットガスの充てんを迅速に行う機構を有することが特長であり，

表2 ガス PET の誤差要因

1．部分容積効果
　放射線濃度の系統的誤差
　動態モデルに依存した誤差伝搬
2．入力関数の遅延と歪みに対する補正誤差
　誤差伝搬を抑制するスキャン時間の設定が必要
3．PET 装置の誤差，不安定性
　PET 装置の誤差，調整不備，etc
　　⇒散乱線補正法の改良
　入力関数モニター装置の誤差（感度の変動，etc）
　Well カウンター装置の不安定さ（energy window のズレ，etc）
4．生理的変動に基づく誤差
　真の変動（$PaCO_2$，Hct，Hb，etc）
　変動に伴う計算誤差
5．操作エラーに基づく誤差
　CCF 操作，採血操作，撮像のタイミング，etc

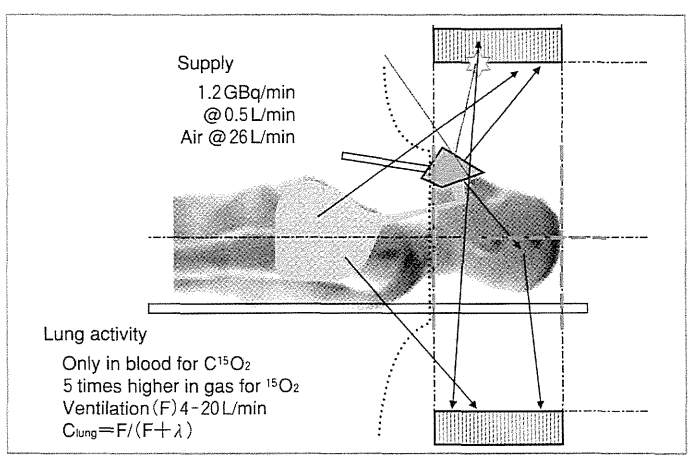

図4 ^{15}O ガス PET における誤差要因
吸入系における強い ^{15}O ガスの影響を排除する工夫が必要である．

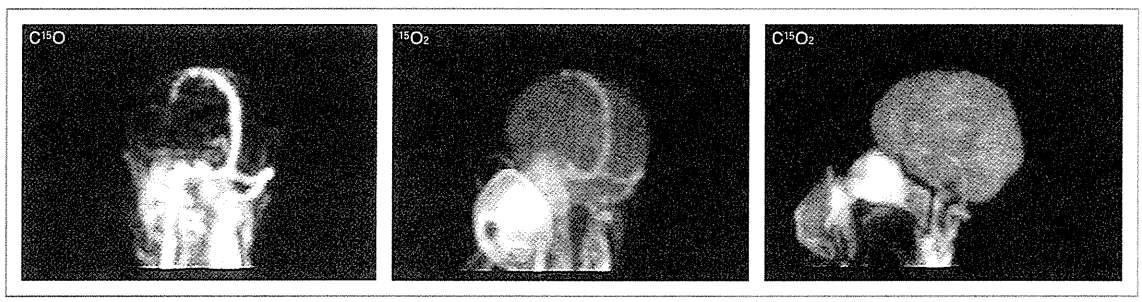

図5 最新の高感度化された3D PET装置で撮像した，$C^{15}O$，$^{15}O_2$，$C^{15}O_2$吸入中の健常者頭部のMIP画像

偶発同時計数，数え落とし，散乱線補正，を正しく補正する物理プロセスを組み込むことで，高感度，高空間解像度，高精度な計測が可能になった．頸動脈などの放射能濃度をモニタするなどの方法を用いることで無採血定量化の可能性が期待される．

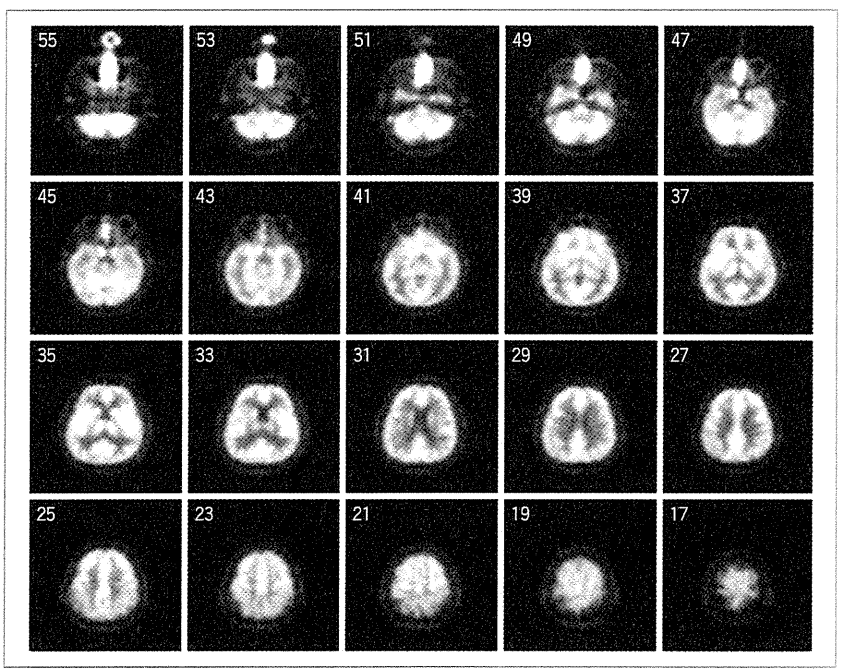

図6 上記3D PETを使って得た健常者の酸素代謝量（定性）画像の例

白質，静脈洞などの分離が鮮明である．

表3 新規^{15}OガスPETシステムにおける改良項目

1．PET画像の精度改善
- 偶発同時係数，数え落とし率の改善
- （3D収集における散乱線補正を含む）
- マスク内放射能の軽減

2．Wellカウンター装置の改良
- Energy windowの確認機能

3．生理的変動に基づく誤差の改善
- マスク内酸素分圧の改善
- 圧迫感の軽減
- 放射性ガスの供給系の安定化
- 検査時間の短縮化

4．手順の軽減
- PETと入力関数の時間調整などの自動化
- 操作の簡便化と作業動線の改善
- 投与量の毎回計測
- 一過性作業の確認機能

医療機器としての装置製造がなされている．さらに^{15}Oガス専用の超小型サイクロトロンと上述の^{15}Oガス合成システムとの組み合わせで，十分な製造能力があることを確認し，それらの一体制御化を試みている．画像解析ワークステーションとの連携，さらに種々の誤差要因を物理的かつソフト的に排除するような工夫（表3）とあわせてシステム構築し，今後有用性と妥当性について検討を行うところである．最終的には，被験者がPET検査室に入室してからの作業動線の効率化，たとえば被験者の固定法やフェースマスクや吸入チューブの装着手順や，$EtCO_2$や血圧，心拍などの生理パラメータのモニタ装置などの接続操作の手順最適化が必要である．このような統合化された検査システムの実用化においては，まさに物理工学研究者と医療スタッフとの共同作業が必要になる．

おわりに

本来，$CMRO_2$は神経細胞のエネルギー代謝を示す指標であり，Mintunら[17]の研究で示されたように，脳組織内の酸素分圧は十分に高いのでCBFは律速段階にはなっていない．一方，CBFは血行力学的な病態だけでなく，種々の神経支配等にも依存して，局所かつグローバルに変化する[18]．このような状況下で脳虚血性疾患におけるOEFやCBF，

$CMRO_2$の絶対値定量化に関する病態論的な意義は必ずしも明らかではない．脳虚血の指標としてのCBFやOEFの絶対値に意義を見出すのであれば，検査環境を限りなく統一化し，同一の生理環境を担保する必要がある．多くの臨床的局面においては，定量数値に意味を見出すのではなく，あくまで局所変化を補足する情報として理解することもひとつの考え方である．真に有用な臨床指標と，それを提示する臨床検査プロトコルについて更なる検討が必要と考えられる．

文献

1) Leenders KL, Perani D, Lammertsma AA, et al: Cerebral blood flow, blood volume and oxygen utilization. Normal values and effect of age. Brain **113** (Pt 1): 27-47, 1990
2) Mintun MA, Raichle ME, Martin WR, et al: Brain oxygen utilization measured with O-15 radiotracers and positron emission tomography. J Nucl Med **25**: 177-187, 1984
3) Iida H, Kanno I, Inugami A, et al: [Continuous-monitoring detector-system of arterial H2(15)O concentration for positron-emission tomography: construction of the system and correction for the dispersion and time-shift]. Kaku igaku The Japanese journal of nuclear medicine **24**: 1587-1594, 1987
4) Kudomi N, Choi E, Yamamoto S, et al: Development of a GSO detector assembly for a continuous blood sampling system. IEEE Trans Nucl Sci **50**: 70-73, 2003
5) Iida H, Higano S, Tomura N, et al: Evaluation of regional differences of tracer appearance time in cerebral tissues using [^{15}O] water and dynamic positron emission tomography. J Cereb Blood Flow Metab **8**: 285-288, 1988
6) Iida H, Kanno I, Miura S, et al: Error analysis of a quantitative cerebral blood flow measurement using $H_2{}^{15}O$ autoradiography and positron emission tomography with respect to the dispersion of the input function. J Cereb Blood Flow Metab **6**: 536-545, 1986
7) Iida H, Jones T, Miura S: Modeling approach to eliminate the need to separate arterial plasma in oxygen-15 inhalation positron emission tomography. J Nucl Med **34**: 1333-1340, 1993
8) Kudomi N, Hayashi T, Watabe H, et al: A physiologic model for recirculation water correction in $CMRO_2$ assessment with $^{15}O_2$ inhalation PET. J Cereb Blood Flow Metab **29**: 355-364, 2009
9) Sasakawa Y, Kudomi N, Yamamoto Y, et al: Omission of [(15)O] CO scan for PET CMRO(2) examination using (15)O-labelled compounds. Ann Nucl Med **25**: 189-196, 2011
10) Ito H, Kanno I, Kato C, et al: Database of normal human cerebral blood flow, cerebral blood volume, cerebral oxygen extraction fraction and cerebral metabolic rate of oxygen measured by positron emission tomography with 15O-labelled carbon dioxide or water, carbon monoxide and oxygen: a multicentre study in Japan. Eur J Nucl Med Mol Imaging **31**: 635-643, 2004
11) Kudomi N, Hayashi T, Teramoto N, et al: Rapid quantitative measurement of $CMRO_2$ and CBF by dual administration of ^{15}O-labeled oxygen and water during a single PET scan-a validation study and error analysis in anesthetized monkeys. J Cereb Blood Flow Metab **25**: 1209-1224, 2005
12) Hattori N, Bergsneider M, Wu HM, et al: Accuracy of a method using short inhalation of (15)O-O(2) for measuring cerebral oxygen extraction fraction with PET in healthy humans. J Nucl Med **45**: 765-770, 2004
13) Yamamoto Y, de Silva R, Rhodes CG, et al: Noninvasive quantification of regional myocardial metabolic rate of oxygen by $^{15}O_2$ inhalation and positron emission tomography. Experimental validation. Circulation **94**: 808-816, 1996
14) Hatazawa J, Fujita H, Kanno I, et al: Regional cerebral blood flow, blood volume, oxygen extraction fraction, and oxygen utilization rate in normal volunteers measured by the autoradiographic technique and the single breath inhalation method. Ann Nucl Med **9**: 15-21, 1995
15) Iida H, Law I, Pakkenberg B, et al: Quantitation of regional cerebral blood flow corrected for partial volume effect using O-15 water and PET: I. Theory, error analysis, and stereologic comparison. J Cereb Blood Flow Metab **20**: 1237-1251, 2000
16) Law I, Iida H, Holm S, et al: Quantitation of regional cerebral blood flow corrected for partial volume effect using O-15 water and PET: II. Normal values and gray matter blood flow response to visual activation. J Cereb Blood Flow Metab **20**: 1252-1263, 2000
17) Mintun MA, Lundstrom BN, Snyder AZ, et al: Blood flow and oxygen delivery to human brain during functional activity: theoretical modeling and experimental data. Proc Natl Acad Sci USA **98**: 6859-6864, 2001
18) Takahashi K: [Regional cerebral blood flow and oxygen consumption during normal human sleep]. No to shinkei = Brain and nerve **41**: 919-925, 1989

Journal of Cerebral Blood Flow & Metabolism (2012) 32, 2066–2075

www.jcbfm.com

Cerebral blood flow and metabolism of hyperperfusion after cerebral revascularization in patients with moyamoya disease

Yasuyuki Kaku[1], Koji Iihara[1], Norio Nakajima[1], Hiroharu Kataoka[1], Kenji Fukuda[1], Jun Masuoka[1], Kazuhito Fukushima[2], Hidehiro Iida[3] and Nobuo Hashimoto[1]

[1]*Department of Neurosurgery, National Cerebral and Cardiovascular Center, Osaka, Japan;* [2]*Department of Radiology, National Cerebral and Cardiovascular Center, Osaka, Japan;* [3]*Department of Investigative Radiology, National Cerebral and Cardiovascular Center Research Institute, Osaka, Japan*

In moyamoya disease (MMD), surgical revascularization may be complicated with postoperative hyperperfusion. We analyzed cerebral perfusion and metabolism using positron emission tomography (PET) or single-photon emission computed tomography (SPECT) before and after bypass surgery on 42 sides of 34 adult patients with MMD. In seven cases (16.7%) with symptomatic hyperperfusion, diagnosed by qualitative ^{123}I-iodoamphetamine (IMP) SPECT, a subsequent PET study during postoperative subacute stages revealed significantly increased cerebral blood flow (CBF) from 34.1 ± 8.2 to 74.3 ± 12.8 mL/100 g per minute ($P < 0.01$), a persistent increase in cerebral blood volume (CBV) from 5.77 ± 1.67 to 7.01 ± 1.44 mL/100 g and a significant decrease in oxygen extraction fraction (OEF) from 0.61 ± 0.09 to 0.40 ± 0.08 ($P < 0.01$). Mean absolute CBF values during symptomatic hyperperfusion were more than the normal control + 2 standard deviations, the predefined criteria of PET. Interestingly, two patients with markedly increased cerebral metabolic rate of oxygen ($CMRO_2$) at hyperperfusion were complicated with postoperative seizure. Among preoperative PET parameters, increased OEF was the only significant risk factor for symptomatic hyperperfusion ($P < 0.05$). This study revealed that symptomatic hyperperfusion in MMD is characterized by temporary increases in CBF > 100% over preoperative values caused by prolonged recovery of increased CBV.
Journal of Cerebral Blood Flow & Metabolism (2012) **32,** 2066–2075; doi:10.1038/jcbfm.2012.110; published online 1 August 2012

Keywords: hyperperfusion; moyamoya disease; positron emission tomography

Introduction

The causes of moyamoya disease (MMD), characterized by progressive stenosis/occlusion of the terminal internal cerebral artery and its branches, are unclear; ischemic and hemorrhage injuries may be the causes of MMD (Suzuki and Takaku, 1969). Superficial temporal artery (STA)-middle cerebral artery (MCA) anastomosis or various kinds of indirect bypasses are recommended for symptomatic patients based on the degree of hemodynamic compromise (Kuroda and Houkin, 2008; Takahashi and Miyamoto, 2010). Despite favorable long-term outcomes after successful bypass surgery for MMD, increasing evidence suggests that this may be complicated with temporary neurologic deterioration during the postoperative acute stage owing to focal cerebral hyperperfusion around the site of the anastomosis (Fujimura *et al*, 2007, 2009, 2011; Furuya *et al*, 2004; Kim *et al*, 2008; Ogasawara *et al*, 2005). Postoperative cerebral hyperperfusion is defined as a major increase in ipsilateral cerebral blood flow (CBF) well above the metabolic demands of brain tissue (Piepgras *et al*, 1988; Sundt *et al*, 1981), and is well characterized in patients after carotid endarterectomy (CEA). Although a similar cerebral hyperperfusion phenomenon was reported in patients with MMD using single-photon emission computed tomography (SPECT) or xenon-enhanced computed tomography (Fujimura *et al*, 2007, 2009, 2011; Furuya *et al*, 2004; Kim *et al*, 2008; Ogasawara *et al*, 2005), no previous study has quantitatively analyzed CBF and metabolism of postoperative hyperperfusion in MMD. The purpose of this study was to analyze CBF and metabolism by positron emission tomography (PET) in cases of symptomatic cerebral hyperperfusion, screened by qualitative

Correspondence: Dr K Iihara, Department of Neurosurgery, National Cerebral and Cardiovascular Center, 5-7-1 Fujishiro-dai Suita, Osaka 565-8565, Japan.
E-mail: kiihara@hsp.ncvc.go.jp
This work was supported by Health Labour Sciences Research Grant from the Ministry of Health, Labour and Welfare of Japan.
Received 10 February 2012; revised 22 May 2012; accepted 4 July 2012; published online 1 August 2012

^{123}I-iodoamphetamine (^{123}I-IMP) SPECT as previously reported, after STA-MCA anastomosis in patients with MMD. Relative increases and absolute values of CBF in PET during symptomatic hyperperfusion in MMD were compared with those of the traditional definition of post CEA hyperperfusion and the predefined CBF value as normal control + 2 standard deviations (s.d.).

Materials and methods

Patient Population

This study protocol was governed by the guidelines of national government based on the Helsinki Declaration revised in 1983, and it was approved by the Institutional Research and Ethics Committee of our hospital. All study participants provided informed consent in the study. Between April 2009 and June 2011, 34 patients (21 women) with MMD were treated at the Department of Neurosurgery, National Cerebral and Cardiovascular Center, Osaka, Japan; age (mean ± s.d.) was 39.3 ± 15.3 years (range, 15 to 70 years). Pediatric patients were excluded from the study. Diagnosis of MMD was based on cerebral angiography studies according to diagnostic criteria updated in 1997 (Fukui, 1997). Presenting symptoms were cerebral infarction ($n = 13$), transient ischemic attack ($n = 24$), involuntary movements ($n = 2$), and intracerebral/intraventricular hemorrhage ($n = 3$). The STA-MCA bypass surgery was performed on 42 hemispheres of these patients.

Surgical Procedure

All patients were treated by the same surgeons (KI and NN). Under general anesthesia mainly using propofol, the parietal and/or frontal branches of the STA were dissected, and single and/or double anastomosis to supra- and/or infra-Sylvian MCA (M4) was performed in a side-to-end manner. The patency of the anastomoses was intraoperatively confirmed by Doppler ultrasonography and indocyanine green videoangiography.

Diagnosis of Symptomatic and Asymptomatic Hyperperfusion Based on Perioperative Positron Emission Tomography and Single-Photon Emission Computed Tomography Studies

The protocol of the perioperative measurement of CBF with/without metabolism was shown in Figure 1. The PET or *N*-isopropyl-*p*-[^{123}I] IMP SPECT was conducted preoperatively (within 1 month of the operation). Preoperative PET was performed mainly for patients with severe ischemic symptoms. As for screening, ^{123}I-IMP SPECT was conducted first during postoperative day (POD) 1 to 3 for all patients to determine qualitatively the presence of a significant focal increase in CBF at the site of anastomosis. Patients associated with other pathologies such as mass effect by the swollen temporal muscle used for indirect anastomosis, subdural/epidural hematoma, and postoperative new frank

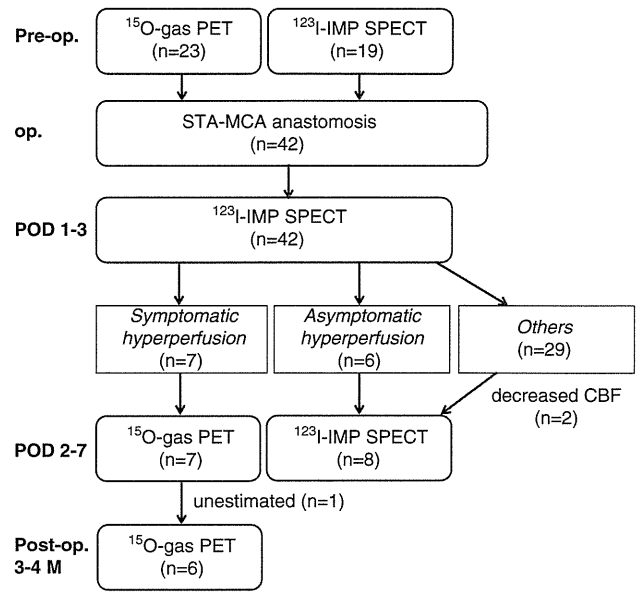

Figure 1 The protocol of the examination. As for screening, ^{123}I-IMP SPECT was conducted first during postoperative day (POD) 1 to 3 for all patients to determine qualitatively the presence of a significant focal increase in cerebral blood flow (CBF) at the site of anastomosis. Then, if patients with hyperperfusion on postoperative ^{123}I-IMP SPECT developed focal neurologic deficits, they underwent the PET study on POD 2 to 7. If patients did not develop new apparent neurologic symptoms despite hyperperfusion on ^{123}I-IMP SPECT, then they were classified as asymptomatic hyperperfusion and repeated the ^{123}I-IMP SPECT study during the subacute stages. Patients with symptomatic hyperperfusion repeated the PET study during the chronic phase 3 to 4 months after surgery. ^{123}I-IMP, ^{123}I-iodoamphetamine; SPECT, single-photon emission computed tomography; PET, positron emission tomography; STA-MCA, superficial temporal artery-middle cerebral artery.

infarction on postoperative diffusion-weighted magnetic resonance (MR) imaging were excluded. Patient with a significant focal increase in CBF at the site of anastomosis on ^{123}I-IMP SPECT were diagnosed as hyperperfusion, as reported previously (Fujimura *et al*, 2007, 2011). Then, if the patients with hyperperfusion on postoperative ^{123}I-IMP SPECT developed focal neurologic deficits related to the perisylvian area (dysarthria, hand motor dysfunction, and motor or sensory dysphasia) and/or severe headache (symptomatic hyperperfusion), they underwent CBF and metabolism measurements with PET during the subacute stage on POD 2 to 7. If patients did not develop new apparent neurologic symptoms despite hyperperfusion on ^{123}I-IMP SPECT, then they were classified as asymptomatic hyperperfusion and repeated the ^{123}I-IMP SPECT study during the subacute stages. The rest of the patients without apparent hyperperfusion on ^{123}I-IMP SPECT did not repeat the ^{123}I-IMP SPECT study unless there was a significant decrease in CBF. Patients with symptomatic hyperperfusion repeated the PET study during the chronic phase 3 to 4 months after surgery. Relative increases in and absolute values of CBF in PET during symptomatic hyperperfusion in MMD were compared with those of the traditional definition of post CEA hyperperfusion (>100% increase

over preoperative CBF values) and the predefined CBF value as normal control + 2s.d.

Positron Emission Tomography Measurement

A series of PET scans were performed to quantitatively assess CBF and cerebral metabolic rate of oxygen ($CMRO_2$) at each stage, according to the dual-tracer autoradiographic protocol developed by Kudomi *et al* (2005) with a minor modification of replacing intravenous administration of ^{15}O-water by ^{15}O-carbondioxide inhalation (Nezu *et al*, 2012). The PET scanner used was ECAT ACCEL from Siemens-CTI (Knoxville, TN, USA), and data were acquired in the 2D mode. The scan can provide an intrinsic spatial resolution of 4.5 mm full-width at half-maximum at the center of the field-of-view. A catheter was placed in the brachial artery for measurement of arterial input function. After a 10-minute transmission scan using a rotating external ^{68}Ge-^{68}Ga rod source, a PET scan was obtained 3 minutes after inhalation of ^{15}O-labeled carbon monoxide gas ($C^{15}O$) of 2,500 MBq for 30 seconds. After the 10 minutes allotted for radioactivity decay, an additional dynamic scan was performed for 8 minutes, while 4,000 MBq of oxygen ($^{15}O_2$) and 5,000 MBq of ^{15}O-labeled carbon dioxide ($C^{15}O_2$) were inhaled through a facemask sequentially at 5-minute intervals. The inhalation period was 1 minute for each gas. Arterial blood was continuously withdrawn during this dynamic scan, and the radioactivity concentration of the blood in the catheter tube was monitored using a scintillator block detector system (BeCON; Molecular Imaging Lab Inc., Suita City, Japan) (Kudomi *et al*, 2003). Arterial blood samples were also taken before and after the dynamic scan, and arterial oxygen content (PO_2) and arterial PCO_2 were measured.

Control values of PET parameters were obtained from eight patients (six male and two female; mean age ± s.d. = 66.1 ± 9.4 years) who had unilateral stenosis of the internal carotid artery or the trunk of MCA with minimal or no infarction on magnetic resonance imaging. Values of PET parameters obtained from the contralateral MCA region were as follows: CBF, 46.6 ± 5.6 mL/100 g per minute; cerebral blood volume (CBV), 2.90 ± 0.61 mL/100 g; $CMRO_2$, 3.56 ± 0.62 mL/100 g per minute; oxygen extraction fraction (OEF), 0.43 ± 0.05; and CBF/CBV, 18.8 ± 6.8/min. There were no significant changes in these values with advancing age.

Single-Photon Emission Computed Tomography Measurement

Preoperative clinical SPECT studies followed the DTARG protocol, with dual administration of iodoamphetamine (Kim *et al*, 2006). Briefly, two dynamic scans were acquired in quick succession, with a 2-minute interval between scans. The first scan covered the initial 0- to 28-minute period and the second was acquired from 30 to 58 minutes. At 4 minutes per frame, seven frames covered each of the two dynamic scan periods. ^{123}I-Iodoamphetamine was infused twice over 1 minute into the antecubital vein at 0 and 30 minutes. Acetazolamide (17 mg/kg, 1,000 mg maximum) was administered intravenously 20 minutes after the first iodoamphetamine injection, corresponding to 10 minutes before the second iodoamphetamine injection. Projection data were summed for the acquisition duration of the first and second scans and reconstructed. The SPECT data provide quantitative information on CBF at rest and after an acetazolamide challenge; it provides information about vascular reserve and the severity of hemodynamic brain ischemia. Regional vascular reserve was defined as the ratio of the difference between acetazolamide-activated regional CBF (rCBF) and resting rCBF to resting rCBF: Regional vascular reserve = ((acetazolamide-activated rCBF/resting rCBF − 1) × 100(%)). The severity of hemodynamic brain ischemia was classified into three stages as follows: stage 0 (vascular reserve > 30%), stage I (30% ⩽ vascular reserve ⩽ 10% or 80% of normal CBF ⩽ resting CBF), and stage II (10% > vascular reserve > −30% and 80% of normal CBF > resting CBF) (JET study Group, 2002). This classification was based on hemodynamic status, determined from PET findings (Powers, 1991). The ^{123}I-IMP autoradiographic method (Iida *et al*, 1994) was performed postoperatively for all patients. The ^{123}I-IMP autoradiographic method uses a single iodoamphetamine administration to assess CBF at rest. The same image reconstruction process as for the DTARG protocol was used.

Magnetic Resonance Imaging Protocol

The MR imaging was performed using a 1.5-T MR scanner (Symphony, Siemens, Erlangen, Germany) fitted with a circularly polarized head coil. Fast fluid-attenuated inversion recovery MR images were acquired before STA-MCA anastomosis (7 ± 5 days before or after the first PET). Sequence parameters were as follows: repetition time/echo time/number of excitations, 9,000 ms/120 ms/1; inversion time, 2,500 ms; turbo factor, 15; and matrix, 352 × 352. Additional MR scans were also performed on each patient during the hyperperfusion phase (1 ± 2 days before or after the second PET) and the chronic phase (7 ± 5 days before or after the third PET).

Data Analysis

The PET images were reconstructed using a standard filtered-back projection technique on the PET scanner console, which included corrections for a scatter and attenuation. A postreconstruction Gaussian filter of 8 mm full-width at half-maximum was also applied. All PET and MR images were then transferred to an independent PC workstation for further analyses. Functional images for CBF, $CMRO_2$, OEF, and CBV were obtained using an in-house program published previously (Kudomi *et al*, 2005), with a minor modification in the process of compensating for the recirculation water in the arterial blood (Iida *et al*, 1993) with automatic separation of two input functions (Kudomi *et al*, 2009). All PET images were registered to the CBF image taken at the preoperative study using Multimodality Image Registration Software (Dr View, AJS Inc., Tokyo, Japan), which fits six rigid body parameters using a mutual information matching technique. The MR images taken at three different time points

were also registered to the CBF image so that all PET and MR images were aligned at the same coordinates. Agreement of the registered images was visually confirmed to match the brain contours between PET and MR images, including the cerebellum, sylvian fissure, and ventricular regions.

Regions-of-interest were carefully selected using QView software from the QSPECT project at National Cerebral and Cardiovascular Center Research Institute (Osaka, Japan) (Iida *et al*, 2010). For quantitative assessment of CBF, $CMRO_2$, OEF, and CBV using PET in patients with symptomatic hyperperfusion, regions-of-interest were constructed to delineate areas of increased CBF around the site of anastomosis on the postoperative PET during the subacute stage compared with preoperative CBF images on PET/SPECT. Regions-of-interest were then superimposed on other PET and MR images. For the rest of the patients in whom preoperative PET was performed, regions-of-interest, consisting of a 1-cm diameter circle along the cortical rim, avoiding the infarcted area, were manually placed over the frontal cortex (targeted to the central area where anastomosis was planned).

Statistical Analysis

All data are presented as the mean ± s.d. All data were analyzed by analysis of variance. If significance was obtained, then we used Scheffe's criteria for multiple comparison. $P < 0.05$ was considered to be significant.

Results

Clinical Characteristics

Preoperative hemodynamic status was categorized using PET and SPECT in 23 (9 sides at stage I and 14 sides at stage II) and 19 (9 sides at stage I and 10 sides at stage II) hemispheres in 34 patients, respectively. In the qualitative ^{123}I-IMP SPECT study on POD 1 to 3, a significant focal increase in CBF at the site of anastomosis was observed in 13 sides (31%), whereas decreased CBF was noted in 2 sides (4.8%). Of the patients with hyperperfusion on qualitative ^{123}I-IMP SPECT, seven sides (16.7%) in six patients became symptomatic (symptomatic hyperperfusion) and subsequently underwent the PET study during POD 2 to 7. The rest of the study population were classified as asymptomatic hyperperfusion in 6 sides (14.3%) and others in 29 sides (69%) based on qualitative ^{123}I-IMP SPECT and the appearance of postoperative new neurologic symptoms (the traditional definition of postoperative hyperperfusion in MMD).

Table 1 presents a summary of the cases with symptomatic hyperperfusion. All patients complicated with symptomatic hyperperfusion presented with ischemic attacks. The incidence of symptomatic hyperperfusion was correlated with the degree of preoperative hemodynamic impairment; 5.9% (1 of 18 sides) at stage I and 25.0% (6 of 24 sides) at stage II. Hyperperfusion on the PET scan was observed in the area near the site of STA-MCA anastomosis. Symptoms related to hyperperfusion included seizure, sensory disturbance, and aphasia in three, two, and two cases, respectively. Symptoms occurred on POD 1 to 4, with the duration being 4 to 14 days. The modified Rankin scale score of patients complicated with symptomatic hyperperfusion was 0 or 1 at postoperative months 3 to 4.

Correlation of Preoperative Positron Emission Tomography Parameters with Symptomatic Hyperperfusion

Table 2 presents preoperative PET parameters in 22 hemispheres of 18 patients. One patient with postoperative decreased CBF on qualitative ^{123}I-IMP SPECT was excluded. These hemispheres were

Table 1 Summary of seven cases in six patients with postoperative symptomatic hyperperfusion

Case no.	*Age, sex*	*Side*	*Onset of MMD*	*Preoperative hemodynamic status*	*Area of hyperperfusion*	*Symptom*	*Onset of hyperperfusion*	*Duration (days)*	*mRS score at 3–4 months*
1	41, F	L	Infarction	Stage II	Precentral and central	Seizure	POD 0	10	1
2	37, M	R	TIA	Stage I[a]	Central and parietal	Seizure	POD 4	4	0
3	44, F	L	Infarction	Stage II	Central	Seizure	POD 3	7	1[b]
4	44, F	R	Infarction	Stage II	Central	Sensory	POD 3	11	1[b]
5	41, F	R	TIA	Stage II	Central	Sensory	POD 3	7	0
6	60, F	L	Infarction	Stage II	Precentral and central	Aphasia	POD 1	11	0
7	51, M	L	TIA	Stage II[a]	Precentral, central, and parietal	Aphasia	POD 3	14	0

^{123}I-IMP, ^{123}I-iodoamphetamine; MMD, moyamoya disease; mRS, modified Rankin Scale; POD, postoperative day; sensory, sensory disturbance; SPECT, single-photon emission computed tomography; TIA, transient ischemic attack.
Case no. 3 and no. 4 were the same patient.
[a]Evaluated by ^{123}I-IMP SPECT.
[b]Resulted from infarction that occurred at the onset of MMD.

Table 2 Preoperative PET parameters in 22 hemispheres of 18 patients

	Postoperative hyperperfusion			P *value*
	Symptomatic	*Asymptomatic*	*Others*	
n	5	4	13	
CBF (mL/100 g per minute)	34.1 ± 8.2	43.2 ± 8.2	33.5 ± 8.8	0.202
CBV (100 g/min)	5.77 ± 1.67	4.63 ± 0.29	4.49 ± 1.06	0.166
$CMRO_2$ (mL/100 g per minute)	3.48 ± 0.51	3.07 ± 0.41	2.92 ± 0.64	0.253
OEF	0.61 ± 0.09	0.44 ± 0.10	0.51 ± 0.08	0.045
CBF/CBV (per minute)	6.7 ± 2.2	9.5 ± 1.6	8.3 ± 2.4	0.236

CBF, cerebral blood flow; CBV, cerebral blood volume; $CMRO_2$, cerebral metabolic rate of oxygen; OEF, oxygen extraction fraction; PET, positron emission tomography.
Values are mean ± s.d.

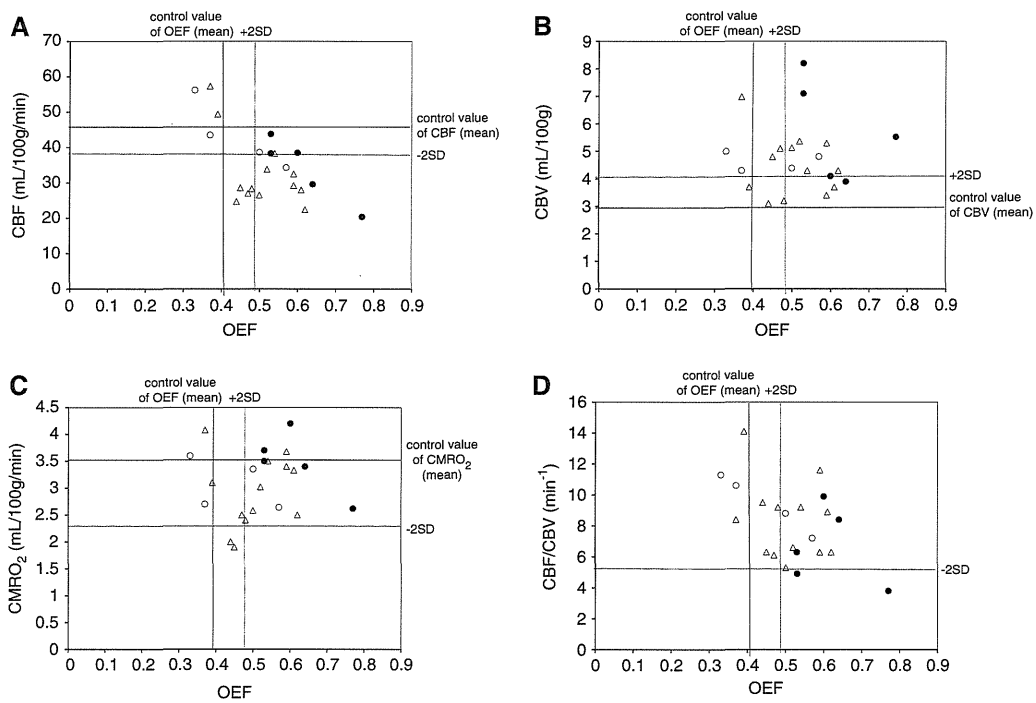

Figure 2 Plot of preoperative absolute values of oxygen extraction fraction (OEF) versus cerebral blood flow (CBF) (**A**), cerebral blood volume (CBV) (**B**), cerebral metabolic rate of oxygen ($CMRO_2$) (**C**), and CBF/CBV (**D**) in 22 hemispheres of 18 patients. Patients were divided by postoperative qualitative ^{123}I-IMP SPECT into three groups: symptomatic hyperperfusion (filled circle), asymptomatic hyperperfusion (open circle), and others (triangle). Solid vertical and horizontal black lines indicate control values of positron emission tomography (PET) parameters and the dotted lines indicate ± 2s.d. for control values of PET parameters, respectively. Four of eight cases with increased OEF and CBV (**B**, upper right quadrant) had postoperative symptomatic hyperperfusion. ^{123}I-IMP, ^{123}I-iodoamphetamine; SPECT, single-photon emission computed tomography.

divided into symptomatic hyperperfusion ($n=5$), asymptomatic hyperperfusion ($n=4$), and others ($n=13$). Although no significant differences in CBF, CBV, $CMRO_2$, and CBF/CBV were found between the three groups, OEF of the hemisphere complicated with symptomatic hyperperfusion was significantly higher than that of the other two groups ($P<0.05$). Relationships between OEF and CBF, CBV, $CMRO_2$, or CBF/CBV were shown in Figure 2. Cases complicated with symptomatic hyperperfusion were almost exclusively noted in those with increased OEF. Of note, four of eight cases (50%) with increased OEF and CBV (Figure 2B, upper right quadrant) had postoperative symptomatic hyperperfusion.

Postoperative Positron Emission Tomography Parameters in Symptomatic Hyperperfusion

Figure 3 illustrates temporal changes in PET parameters in seven hemispheres of six patients with postoperative hyperperfusion. The CBF values in patients with postoperative hyperperfusion significantly increased from the preoperative baseline value of 34.1 ± 8.2 mL/100 g per minute ($n=5$) to

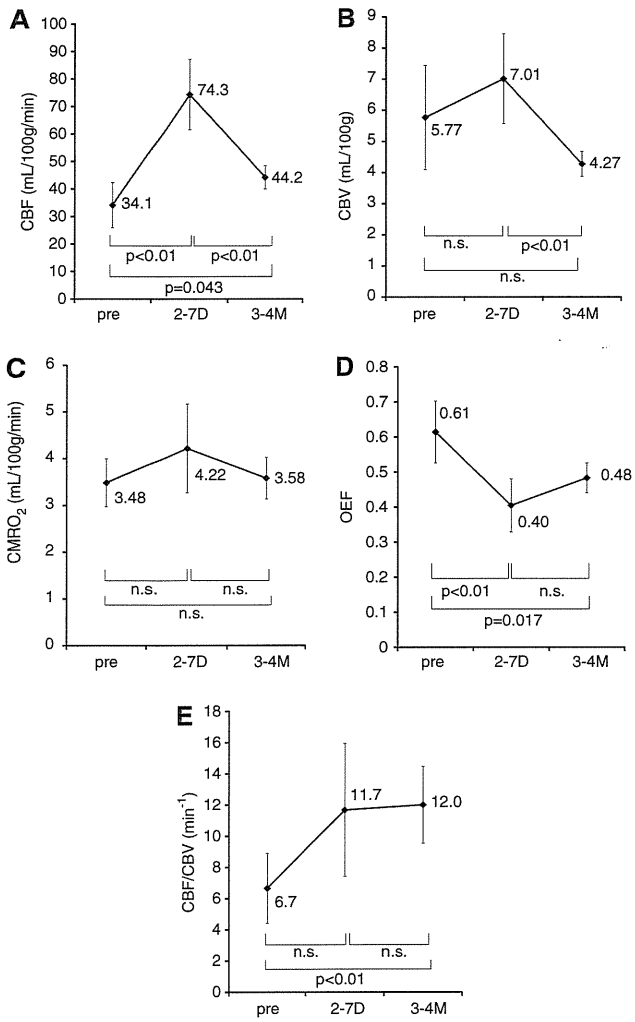

Figure 3 Graphs showing sequential changes in cerebral blood flow (CBF) (**A**), cerebral blood volume (CBV) (**B**), cerebral metabolic rate of oxygen ($CMRO_2$) (**C**), oxygen extraction fraction (OEF) (**D**), and CBF/CBV (**E**) at three different time points: preoperative (pre), subacute postoperative (2 to 7 days (2-7D)), and chronic postoperative (3 to 4 months (3-4M)). Mean values ± standard deviation are shown.

74.3 ± 12.8 mL/100 g per minute ($n = 7$) at the time of hyperperfusion during the subacute stage, and returned to normal levels 3 to 4 months postoperatively (Figure 3A). The preoperative increase in CBV (5.77 ± 1.67 mL/100 g) persisted (7.01 ± 1.44 mL/100 g) during hyperperfusion (normal + 2s.d., 4.12 mL/100 g), and decreased 3 to 4 months postoperatively (Figure 3B). In contrast to interval changes in CBF, $CMRO_2$ increased from 3.48 ± 0.51 to 4.22 ± 0.95 mL/100 g per minute during postoperative hyperperfusion. Interestingly, $CRMO_2$ remained within normal ranges even during hyperperfusion at a peak of 71% (5/7) in the patients. However, the two remaining cases with markedly increased $CMRO_2$ were complicated with postoperative seizures (Figure 3C). As a result, OEF decreased significantly from 0.61 ± 0.09 at baseline to 0.40 ± 0.08 during hyperperfusion (Figure 3D). Cerebral perfusion pressure (CBF/CBV) increased from 6.7 ± 2.2 to 11.7 ± 4.3/min during the subacute stage (Figure 3E). During the follow-up period, values for CBF, $CMRO_2$, and OEF returned to normal levels, while CBV and CBF/CBV showed an improvement over compared with the preoperative values in the region with postoperative hyperperfusion.

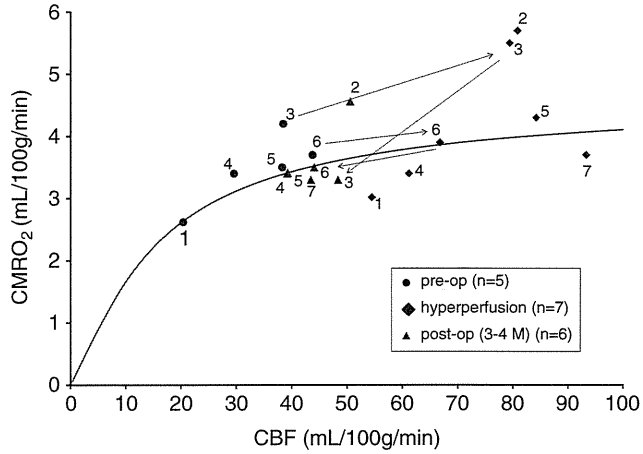

Figure 4 Graph showing the correlation between cerebral blood flow (CBF) and cerebral metabolic rate of oxygen ($CMRO_2$). The Renkin–Crone model (Crone, 1963; Renkin, 1959) was applied to the relationship between CBF and $CMRO_2$. The fitted curve shows that increases in flow lead to smaller changes in $CMRO_2$. The relationship between CBF and $CMRO_2$ almost fits the model for all cases, with the exception of two cases with postoperative seizure, in which the plots were above the curve. Number indicated the case number, respectively.

Comparison of Cerebral Blood Flow with Cerebral Metabolic Rate of Oxygen

Figure 4 shows the correlation between $CMRO_2$ and CBF. The simulated curve shows that increases in CBF lead to smaller changes in $CMRO_2$. Applying the Renkin–Crone model (Crone, 1963; Renkin, 1959) to the relationship between $CMRO_2$ and CBF, the best equation fitting our data for this relationship between them was

$$CMRO_2 = CBF \times OEF = CBF \times (1 - e^{-0.26/CBF}) \quad (1)$$

The fitted curve (Figure 4) showed that the increase in $CMRO_2$ was linear until a flow of ~30 mL/100 g per minute was achieved, and it then increased more gradually as the flow increased. The relationship between CBF and $CMRO_2$ almost fits the Rankin–Crone model (Crone, 1963; Renkin, 1959) with the exception of two cases with postoperative seizure, in which the plots were above the curve.

Representative Case

A 41-year-old woman (case 5) experienced a transient ischemic attack of left-sided sensory disturbance for

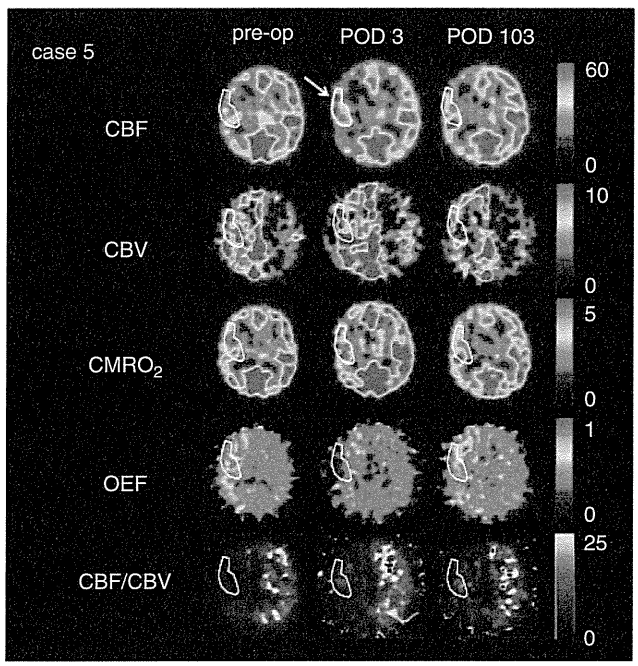

Figure 5 A series of positron emission tomography (PET) studies of a moyamoya disease (MMD) patient (case 5) with symptomatic hyperperfusion. Left: preoperative examinations revealed severe hypoperfusion in the right hemisphere with markedly increased cerebral blood volume (CBV) and oxygen extraction fraction (OEF). CBF/CBV was markedly decreased. Middle: studies obtained on postoperative day 3 showing a marked increase in CBF (white arrow), with persistent increased CBV. Although cerebral metabolic rate of oxygen ($CMRO_2$) was slightly increased, OEF markedly decreased. Right: postoperative examinations obtained 3 months after revascularization. CBF, $CMRO_2$, and OEF were normalized, and CBV and CBF/CBV were improved over the preoperative status. CBF, cerebral blood flow; POD, postoperative day.

a few minutes 5 years ago, and her symptoms gradually worsened. Neuroradiologic examinations showed typical findings compatible with MMD. A PET study indicated misery perfusion on the right hemisphere (Figure 5). The STA-MCA bypass surgery was performed successfully, and she awoke from anesthesia without neurologic deficits. On the third POD, sensory disturbance lasting 30 minutes occurred; similar episodes were repeated several times until the seventh POD. A PET study on POD 3 showed increased CBF and decreased OEF around the anastomotic site. Symptomatic hyperperfusion was diagnosed and her blood pressure was carefully monitored and controlled. Symptoms spontaneously resolved, and the patient was discharged on POD 10.

Discussion

Hyperperfusion Syndrome

Recently, cerebral hyperperfusion has received much attention as a possible cause of transient neurologic dysfunction after bypass surgery for MMD. The main neurologic deficits corresponding to dysfunctions around the bypass site at the perisylvian area include dysarthria, hand motor dysfunction, and motor or sensory dysphasia. Unlike the classical triad of symptoms such as severe unilateral headache, face and eye pain, and seizures and established criteria of CBF after CEA (Piepgras *et al*, 1988; Sundt *et al*, 1981; van Mook *et al*, 2005), a critical definition of CBF using PET, a gold standard, for the diagnosis of hyperperfusion after bypass surgery for MMD remains unestablished.

Here the authors reported, for the first time in MMD, CBF and oxygen metabolism with preoperative and postoperative PET, after screening patients with hyperperfusion first with qualitative ^{123}I-IMP SPECT, the reported definition of postoperative hyperperfusion in MMD, and analyzed the correlation of preoperative PET parameters with development of symptomatic hyperperfusion, and found that preoperative OEF was significantly increase in the patients, whereas no differences were observed in the other parameters. A postoperative PET study, exclusively performed for cases with symptomatic hyperperfusion due to difficult logistic reasons, clearly showed that transient neurologic deterioration due to hyperperfusion was characterized by transient increases in CBF caused by prolonged recovery of CBV, as reported previously in hyperperfusion after CEA and carotid artery stenting (CAS). In terms of oxygen metabolism, however, patients with hyperperfusion were classified into two types, those with normal and elevated $CMRO_2$, respectively, and the latter type was complicated with postoperative seizure.

Diagnosis of Symptomatic Hyperperfusion in Moyamoya Disease

In MMD patients, the incidence of symptomatic hyperperfusion after bypass surgery varies considerably from 21.5% to 38.2% (Fujimura *et al*, 2007, 2011), because of a lack of quantitative evaluation of postoperative CBF and different study populations. Unlike hyperperfusion after CEA, the operational definition of hyperperfusion after bypass surgery for MMD remains unestablished. In this paper, qualitative ^{123}I-IMP SPECT was conducted first during POD 1 to 3 to screen all patients for the presence of hyperperfusion according to the previously reported diagnostic criteria of postoperative hyperperfusion in MMD. The incidence of hyperperfusion on qualitative ^{123}I-IMP SPECT (31%) and symptomatic hyperperfusion (16.7%) in the present study was consistent with the previous report.

Here, the postoperative PET study clearly showed that once symptomatic, mean CBF values increased to 218% of preoperative values, which seems to be consistent with the original concept of post CEA perfusion, and peak CBF values at the subacute postoperative stage were equal to or more than the

control + 2s.d. (57.8 mL/100 g per minute), the predefined value of hyperperfusion on PET calculated from the healthy hemisphere in patients with unilateral stenoocclusive lesions in all cases (Fink *et al*, 1993). This definition based on normal control values seems to be practical since preoperative CBF values on PET may not always be available because of inherent logistic difficulties as in the present study. Taken together, these results indicated that if patients with increased CBF on qualitative ^{123}I-IMP SPECT develop corresponding symptoms postoperatively (the previously reported definition of symptomatic hyperperfusion), peak CBF values measured using PET during subacute stages would be almost consistent with the traditional concept of post CEA hyperperfusion (>100% increase over the baseline) and more than predefined CBF threshold values (control + 2s.d.). The CBF values 3 to 4 months postoperatively remained higher than preoperative values, but returned to normal ranges, indicating that the state of hyperperfusion was temporary.

Mechanism of Hyperperfusion in Moyamoya Disease

Preoperative increases in CBV persisted during hyperperfusion and decreased 3 to 4 months postoperatively, suggesting the prolonged recovery of high CBV values, despite immediate increases in perfusion pressure after direct bypass, may have a key role in the development of hyperperfusion and the associated clinical symptoms lasting for 1 to 14 days in our patients. Accordingly, the preoperative decreased cerebral perfusion pressure increased rapidly within 2 to 7 days of surgery. However, the only PET study on postoperative hyperperfusion after CAS (Matsubara *et al*, 2009) showed significant increases in CBF and CBF/CBV ratios despite the lack of significant changes in CBV during the acute stage. Interestingly, such PET findings were observed in the contralateral hemisphere during the acute stage after CAS. Such differences in temporal changes of PET parameters between MMD and CAS are probably explained by the types of revascularization (high flow or low flow), presence of intracranial arterial stenosis in MMD, and the fact that our study on symptomatic MMD mainly consisted of cases with severe hemodynamic compromise than the CAS PET study (Matsubara *et al*, 2009). Therefore, fundamental mechanisms underlying postoperative hyperperfusion, prolonged recovery of vascular reserve, after bypass surgery for MMD seem to be similar to those after carotid revascularization, although the PET study on carotid stenosis with severe hemodynamic compromise is mandatory to conclude this point. Stringent blood pressure control is similarly necessary for patients with postoperative hyperperfusion in MMD (Fujimura *et al*, 2011), although the blood pressure-lowering effect on the untreated contralateral hemisphere should be carefully considered.

Risk of Symptomatic Hyperperfusion

Decreased vascular reserve on preoperative SPECT images has been reported as a predictor of hyperperfusion syndrome after CEA (Hosoda *et al*, 2001; Ogasawara *et al*, 2003). Cerebral perfusion pressure is generally considered to reflect cerebral vascular reserve and the CBF/CBV ratio is an index of cerebral perfusion pressure (Gibbs *et al*, 1984). Cerebral blood volume is closely related to arteriolar dilatation (Kontos *et al*, 1977; Wahl *et al*, 1970) in response to decreased perfusion pressure distal to hemodynamically significant arterial stenosis. Here, we showed among the preoperative PET parameters that increased OEF was the only significant risk factor for the development of symptomatic hyperperfusion. Also, it is interesting to note that although not significantly different, CBV values tended to be higher in symptomatic hyperperfusion. In this context, Derdeyn *et al* (2002) reported the revised concept of hemodynamic staging using PET and showed that among patients with increased OEF, those with increased CBV may indicate pronounced vasodilatation due to exhausted autoregulatory vasodilatation and be associated with a higher risk of subsequent stroke, whereas those with normal CBV may reflect preserved autoregulatory capacity and be associated with a smaller incidence of subsequent stroke. Taken together, our observations presented in Figure 2B may indicate that even in patients with increased OEF, preoperative increased CBV confers a higher risk of symptomatic hyperperfusion than those with normal CBV. Further studies are necessary to conclude this point.

Cerebral Oxygen Metabolism of Hyperperfusion

The present series consisted of patients with preoperative moderate/severe hemodynamic compromise, and temporary clamping of the recipient arteries may confer additional ischemic insult to the brain adjacent to the anastomotic site during bypass. Previous PET studies in patients with cerebral infarctions showed that rapid perfusion to a cerebrum that has been in a state of chronic ischemia may increase oxygen mechanism (postischemic oxygen hypermetabolism) (Marchal *et al*, 1996, 1999). The postulated mechanisms are (1) overexcitation of cellular metabolism in cells destined to survive or (2) excessive firing of neurons undergoing irreversible damage from a massive release of excitatory amino acids during the period of ischemia or early noxious inflammatory changes. Since no frank infarctions were noted in the area with hyperperfusion on magnetic resonance imaging in subacute or chronic periods in the present study, the above-mentioned overexcitation of cellular metabolism cannot be ruled out as a mechanism underlying postoperative hyperperfusion.

Repetitive neurologic symptoms in patients without overt postoperative convulsion may be caused by

partial seizure. Postoperative seizure is considered to be caused by two basic mechanisms; free radical generation mainly caused by extravascular leakage of blood components, and disturbance of ionic balances across the cell membrane caused by ischemia or hypoxia, both of which are closely linked (Manaka *et al*, 2003). Since postoperative hyperperfusion and seizure share two common underlying mechanisms, that is, free radical generation and ischemic insult, the causal relationship between these two phenomena is difficult to answer conclusively based on this study.

Significant oxygen hypermetabolism was noted only in cases complicated with postoperative seizure. Seizure is an abnormal physiological state that, unlike somatosensory processing, places supranormal demands on autoregulatory mechanisms due to an enormous increase in $CMRO_2$ (Folbergrova *et al*, 1981). During sustained seizures, CBF increases with a corresponding increase in $CMRO_2$ (Brodersen *et al*, 1973; Theodore *et al*, 1996). Our analysis using the Renkin–Crone model (Crone, 1963; Renkin, 1959) showed, with the exception of two cases complicated with seizure, there was no mismatch with CBF and $CMRO_2$. The increased tendency of oxygen hypermetabolism during symptomatic hyperperfusion compared with preoperative or chronic periods even in cases without postoperative seizure was also shown in hyperperfusion after CAS (Matsubara *et al*, 2009). Such oxygen hypermetabolism may explain the sustained neurologic deterioration after bypass surgery for MMD.

Conclusion

This study revealed that symptomatic hyperperfusion in MMD is characterized by temporary increases in CBF >100% over preoperative values caused by prolonged recovery of increased CBV. Among preoperative PET parameters, increased OEF was the only significant risk factor for symptomatic hyperperfusion ($P<0.05$). The causal relationship between seizures and increased $CMRO_2$ during symptomatic hyperperfusion remains unknown.

Disclosure/conflict of interest

The authors declare no conflict of interest.

References

Brodersen P, Paulson OB, Bolwig TG, Rogon ZE, Rafaelsen OJ, Lassen NA (1973) Cerebral hyperemia in electrically induced epileptic seizures. *Arch Neurol* 28:334–8

Crone C (1963) The permeability of capillaries in various organs as determined by use of the 'indicator diffusion' method. *Acta Physiol Scand* 58:292–305

Derdeyn CP, Videen TO, Yundt KD, Fritsch SM, Carpenter DA, Grubb RL, Powers WJ (2002) Variability of cerebral blood volume and oxygen extraction: stages of cerebral haemodynamic impairment revisited. *Brain* 125:595–607

Fink GR, Herholz K, Pietrzyk U, Huber M, Heiss WD (1993) Peri-infarct perfusion in human ischemia: Its relation to tissue metabolism, morphology, and clinical outcome. *J Stroke Cerebrovasc Dis* 3:123–31

Folbergrova J, Ingvar M, Siesjo BK (1981) Metabolic changes in cerebral cortex, hippocampus, and cerebellum during sustained bicuculline-induced seizures. *J Neurochem* 37:1228–38

Fujimura M, Kaneta T, Mugikura S, Shimizu H, Tominaga T (2007) Temporary neurologic deterioration due to cerebral hyperperfusion after superficial temporal artery-middle cerebral artery anastomosis in patients with adult-onset moyamoya disease. *Surg Neurol* 67: 273–82

Fujimura M, Mugikura S, Kaneta T, Shimizu H, Tominaga T (2009) Incidence and risk factors for symptomatic cerebral hyperperfusion after superficial temporal artery-middle cerebral artery anastomosis in patients with moyamoya disease. *Surg Neurol* 71:442–7

Fujimura M, Shimizu H, Inoue T, Mugikura S, Saito A, Tominaga T (2011) Significance of focal cerebral hyperperfusion as a cause of transient neurologic deterioration after extracranial-intracranial bypass for moyamoya disease: comparative study with non-moyamoya patients using N-isopropyl-p-[(123)I]iodoamphetamine single-photon emission computed tomography. *Neurosurgery* 68:957–64; discussion 64–5

Fukui M (1997) Guidelines for the diagnosis and treatment of spontaneous occlusion of the circle of Willis ('moyamoya' disease). Research Committee on Spontaneous Occlusion of the Circle of Willis (Moyamoya Disease) of the Ministry of Health and Welfare, Japan. *Clin Neurol Neurosurg* 99(Suppl 2):S238–40

Furuya K, Kawahara N, Morita A, Momose T, Aoki S, Kirino T (2004) Focal hyperperfusion after superficial temporal artery-middle cerebral artery anastomosis in a patient with moyamoya disease. Case report. *J Neurosurg* 100:128–32

Gibbs JM, Leenders KL, Wise RJ, Jones T (1984) Evaluation of cerebral perfusion reserve in patients with carotid-artery occlusion. *Lancet* 1:182–6

Hosoda K, Kawaguchi T, Shibata Y, Kamei M, Kidoguchi K, Koyama J, Fujita S, Tamaki N (2001) Cerebral vasoreactivity and internal carotid artery flow help to identify patients at risk for hyperperfusion after carotid endarterectomy. *Stroke* 32:1567–73

Iida H, Itoh H, Nakazawa M, Hatazawa J, Nishimura H, Onishi Y, Uemura K (1994) Quantitative mapping of regional cerebral blood flow using iodine-123-IMP and SPECT. *J Nucl Med* 35:2019–30

Iida H, Jones T, Miura S (1993) Modeling approach to eliminate the need to separate arterial plasma in oxygen-15 inhalation positron emission tomography. *J Nucl Med* 34:1333–40

Iida H, Nakagawara J, Hayashida K, Fukushima K, Watabe H, Koshino K, Zeniya T, Eberl S (2010) Multicenter evaluation of a standardized protocol for rest and acetazolamide cerebral blood flow assessment using a quantitative SPECT reconstruction program and split-dose 123I-iodoamphetamine. *J Nucl Med* 51:1624–31

JET Study Group (2002) Japanese EC-IC bypass Trial (JET study): study design and analysis. *Surg Cerebral Stroke* 30:97–100

Kim JE, Oh CW, Kwon OK, Park SQ, Kim SE, Kim YK (2008) Transient hyperperfusion after superficial tem-

poral artery/middle cerebral artery bypass surgery as a possible cause of postoperative transient neurological deterioration. *Cerebrovasc Dis* 25:580–6

Kim KM, Watabe H, Hayashi T, Hayashida K, Katafuchi T, Enomoto N, Ogura T, Shidahara M, Takikawa S, Eberl S, Nakazawa M, Iida H (2006) Quantitative mapping of basal and vasareactive cerebral blood flow using split-dose 123I-iodoamphetamine and single photon emission computed tomography. *Neuroimage* 33:1126–35

Kontos HA, Raper AJ, Patterson JL (1977) Analysis of vasoactivity of local pH, PCO2 and bicarbonate on pial vessels. *Stroke* 8:358–60

Kudomi N, Choi E, Yamamoto S, Watabe H, Kim K, Shidahara M, Ogawa M, Teramoto N, Sakamoto E, Iida H (2003) Development of a GSO detector assembly for a continuous blood sampling system. *IEEE Trans Nucl Sci* 50:70–3

Kudomi N, Hayashi T, Teramoto N, Watabe H, Kawachi N, Ohta Y, Kim KM, Iida H (2005) Rapid quantitative measurement of $CMRO_2$ and CBF by dual administration of ^{15}O-labeled oxygen and water during a single PET scan—a validation study and error analysis in anesthetized monkeys. *J Cereb Blood Flow Metab* 25: 1209–24

Kudomi N, Hayashi T, Watabe H, Teramoto N, Piao R, Ose T, Koshino K, Ohta Y, Iida H (2009) A physiologic model for recirculation water correction in $CMRO_2$ assessment with $^{15}O_2$ inhalation PET. *J Cereb Blood Flow Metab* 29:355–64

Kuroda S, Houkin K (2008) Moyamoya disease: current concepts and future perspectives. *Lancet Neurol* 7:1056–66

Manaka S, Ishijima B, Mayanagi Y (2003) Postoperative seizures: epidemiology, pathology, and prophylaxis. *Neurol Med Chir* 43:589–600

Marchal G, Furlan M, Beaudouin V, Rioux P, Hauttement JL, Serrati C, de la Sayette V, Le Doze F, Viader F, Derlon JM, Baron JC (1996) Early spontaneous hyperperfusion after stroke. A marker of favourable tissue outcome? *Brain* 119(Part 2):409–19

Marchal G, Young AR, Baron JC (1999) Early postischemic hyperperfusion: pathophysiologic insights from positron emission tomography. *J Cereb Blood Flow Metab* 19:467–82

Matsubara S, Moroi J, Suzuki A, Sasaki M, Nagata K, Kanno I, Miura S (2009) Analysis of cerebral perfusion and metabolism assessed with positron emission tomography before and after carotid artery stenting. *J Neurosurg* 111:28–36

Nezu T, Yokota C, Uehara T, Yamauchi M, Fukushima K, Toyoda K, Matsumoto M, Iida H, Minematsu K (2012) Preserved acetazolamide reactivity in lacunar patients with severe white-matter lesions: ^{15}O labeled gas and H_2O positron emission tomography studies. *J Cereb Blood Flow Metab* 32:844–50

Ogasawara K, Komoribayashi N, Kobayashi M, Fukuda T, Inoue T, Yamadate K, Ogawa A (2005) Neural damage caused by cerebral hyperperfusion after arterial bypass surgery in a patient with moyamoya disease: case report. *Neurosurgery* 56:E1380

Ogasawara K, Yukawa H, Kobayashi M, Mikami C, Konno H, Terasaki K, Inoue T, Ogawa A (2003) Prediction and monitoring of cerebral hyperperfusion after carotid endarterectomy by using single-photon emission computerized tomography scanning. *J Neurosurg* 99: 504–10

Piepgras DG, Morgan MK, Sundt TM, Jr, Yanagihara T, Mussman LM (1988) Intracerebral hemorrhage after carotid endarterectomy. *J Neurosurg* 68:532–6

Powers WJ (1991) Cerebral hemodynamics in ischemic cerebrovascular disease. *Ann Neurol* 29:231–40

Renkin EM (1959) Transport of potassium-42 from blood to tissue in isolated mammalian skeletal muscles. *Am J Physiol* 197:1205–10

Sundt TM, Jr, Sharbrough FW, Piepgras DG, Kearns TP, Messick JM, Jr, O'Fallon WM (1981) Correlation of cerebral blood flow and electroencephalographic changes during carotid endarterectomy: with results of surgery and hemodynamics of cerebral ischemia. *Mayo Clin Proc* 56:533–43

Suzuki J, Takaku A (1969) Cerebrovascular 'moyamoya' disease. Disease showing abnormal net-like vessels in base of brain. *Arch Neurol* 20:288–99

Takahashi JC, Miyamoto S (2010) Moyamoya disease: recent progress and outlook. *Neurol Med Chir (Tokyo)* 50: 824–32

Theodore WH, Balish M, Leiderman D, Bromfield E, Sato S, Herscovitch P (1996) Effect of seizures on cerebral blood flow measured with ^{15}O-H_2O and positron emission tomography. *Epilepsia* 37:796–802

van Mook WN, Rennenberg RJ, Schurink GW, van Oostenbrugge RJ, Mess WH, Hofman PA, de Leeuw PW (2005) Cerebral hyperperfusion syndrome. *Lancet Neurol* 4:877–88

Wahl M, Deetjen P, Thurau K, Ingvar DH, Lassen NA (1970) Micropuncture evaluation of the importance of perivascular pH for the arteriolar diameter on the brain surface. *Pflugers Arch* 316:152–63

Journal of Cerebral Blood Flow & Metabolism (2012) 32, 1757–1764

www.jcbfm.com

Reproducibility of cerebral blood flow assessment using a quantitative SPECT reconstruction program and split-dose ^{123}I-iodoamphetamine in institutions with different γ-cameras and collimators

Hiroshi Yoneda[1], Satoshi Shirao[1], Hiroyasu Koizumi[1], Fumiaki Oka[1], Hideyuki Ishihara[1], Kunitsugu Ichiro[2], Tetsuhiro Kitahara[3], Hidehiro Iida[4] and Michiyasu Suzuki[1]

[1]*Department of Neurosurgery and Clinical Neuroscience, Yamaguchi University School of Medicine, Yamaguchi, Japan;* [2]*Department of Public Health, Yamaguchi University School of Medicine, Yamaguchi, Japan;* [3]*Department of Neurosurgery, Ogori Daiichi General Hospital, Yamaguchi, Japan;* [4]*Department of Biomedical Imaging Advanced Medical Engineering Division, National Cerebral and Cardiovascular Center-Research Institute, Osaka, Japan*

Single photon emission computed tomography (SPECT) is used widely in clinical studies. However, the technique requires image reconstruction and the methods for correcting scattered radiation and absorption are not standardized among SPECT procedures. Therefore, quantitation of cerebral blood flow (CBF) may not be constant across SPECT models. The quantitative SPECT (QSPECT) software package has been developed for standardization of CBF. Using the QSPECT/dual-table autoradiographic (DTARG) method, CBF and cerebral vascular reactivity (CVR) at rest and after acetazolamide challenge can be evaluated using ^{123}I-iodoamphetamine in a single SPECT session. In this study, we examined the reproducibility of quantitative regional CBF and CVR in QSPECT/DTARG using different SPECT models at two facilities. The subjects were nine patients with chronic cerebral ischemic disease who underwent QSPECT/DTARG at both facilities with use of different γ-cameras and collimators. There were significant correlations for CBF at rest and after acetazolamide challenge measured at the two facilities. The consistency of the CBFs of the patients measured at the two facilities were good in all cases. Our results show that CBF measured by QSPECT/DTARG in the same patients is reproducible in different SPECT models. This indicates that standardized evaluation of CBF can be performed in large multicenter studies.
Journal of Cerebral Blood Flow & Metabolism (2012) **32,** 1757–1764; doi:10.1038/jcbfm.2012.67; published online 23 May 2012

Keywords: cerebral blood flow; ^{123}I-iodoamphetamine; quantitation; SPECT; vascular reactivity

Introduction

Several imaging modalities for measurement of cerebral circulation have been developed, including positron emission tomography (PET), single photon emission computed tomography (SPECT), perfusion CT, Xe-CT, perfusion magnetic resonance imaging, ultrasonography, and near-infrared spectroscopy. Among these techniques, ^{15}O-PET is excellent in terms of quantitation and space resolution (Frackowiak *et al*, 1980) and can detect the severity of hemodynamic cerebral ischemia as the rise of the oxygen extraction fraction (OEF) (Yamauchi *et al*, 1999). An elevated OEF is defined as misery perfusion (Yamauchi *et al*, 1999), which may be a risk for recurrent stroke and a cause of selective neuronal damage in patients with major cerebral arterial occlusive disease. Therefore, evaluation of the severity of cerebral ischemia is important in predicting prognosis and determining the therapeutic strategy (Yamauchi *et al*, 2007). Ideally, all patients with ischemic cerebrovascular disease should be assessed by PET, but this is impractical because PET facilities are limited. In contrast, SPECT is more commonly available and has broader versatility than PET. Therefore, the use of SPECT for evaluation of the severity of cerebral ischemia could have significant benefits for more patients with ischemic cerebrovascular disorders.

Correspondence: Dr H Yoneda, Department of Neurosurgery and Clinical Neuroscience, Yamaguchi University School of Medicine, 1-1-1 Minami-kogushi, Ube, Yamaguchi 755-8505, Japan.
E-mail: h-yoneda@yamaguchi-u.ac.jp
Received 16 August 2011; revised 3 May 2012; accepted 3 May 2012; published online 23 May 2012

Single photon emission computed tomography cannot be used to observe OEF directly, but quantitation of cerebral blood flow (CBF) using the *N*-isopropy1-[^{123}I]p-iodoamphetamine (IMP) autoradiographic (ARG) method (Hatazawa *et al*, 1997; Iida *et al*, 1994, 1996) can be used to measure thresholds for CBF at rest, determine the cerebrovascular reserve, and detect misery perfusion (Hirano *et al*, 1994). Moreover, the development of the Dual-Table ARG (DTARG) method has made it possible to evaluate CBF at rest and to determine cerebral vascular reactivity (CVR) after acetazolamide challenge using ^{123}I-IMP in a single day session (Kim *et al*, 2006). However, the reproducibility of these methods and standardization among different SPECT models have not been established. In particular, SPECT has a perceived problem that different models of γ-cameras and collimators may give different quantitative values. Therefore, standardization among models and ensuring reproducibility of measured values would be big steps towards utilizing the versatility of SPECT.

To address these issues, QSPECT (quantitative SPECT image reconstruction) has been developed as a program that automatically and accurately corrects attenuated absorption and scattered radiation (Iida *et al*, 1998). This program has been combined with DTARG to give the QSPECT/DTARG method (Iida *et al*, 2010; Kim *et al*, 2006). However, the reproducibility and errors of CBF and CVR measured in the same patients with different SPECT models using QSPECT/DTARG have not been evaluated. In this study, we retrospectively analyzed QSPECT/DTARG data for patients treated at Yamaguchi University Hospital (hereinafter referred to as institution Y) and its affiliated hospital, Ogori Daiichi General Hospital (institution O). These two institutions use different models of γ-cameras and collimators for SPECT, and this provided an opportunity for validation of the reproducibility and determination of the errors of the measured values.

Patients and methods

Patients

The study had a noninterventional, crosssectional design. The protocol was approved by the Yamaguchi University Hospital Institutional Review Board (No. H22-19) and followed the principles of the Declaration of Helsinki. All patient information was anonymized and protected. Among patients who received medical treatment at institution O from September 2005 to August 2009 and were diagnosed with chronic cerebral infarction with cerebrovascular stenosis and underwent QSPECT/DTARG, 25 patients required surgical revascularization and were referred to institution Y, at which QSPECT/DTARG was performed again. Among the 25 patients, 9 (five males and four females) had no differences in medications or clinical conditions at the times QSPECT/DTARG was performed at both facilities. The other 16 patients received additional administration of cilostazol, an antithrombotic agent, before the SPECT examination at institution Y. One of these patients was also treated with pioglitazone for diabetes. Cilostazol and pioglitazone may both increase CBF (Kai *et al*, 2011; Matsumoto *et al*, 2011; Sato *et al*, 2011). Therefore, the 16 patients who received these drugs before the second SPECT examination were excluded because the drugs might have affected the quantitative reproducibility in the study.

Values of CBF in the middle cerebral artery (MCA) territories at rest and after acetazolamide challenge measured at both facilities were examined in these nine patients.

Iodoamphetamine Single Photon Emission Computed Tomography Study Protocol

Procedures for QSPECT/DTARG (Iida *et al*, 2010) are shown in Figure 1. In institution Y, SPECT was performed with a three-headed $\tilde{\alpha}$-camera (GCA-9300A/PI; Toshiba Medical Systems, Tokyo, Japan) and a LESHR fan beam collimator (Toshiba Medical Systems). The energy range was centered at 160 keV with a width of 20%, and 2-minute rotation was performed 14 times in continuous mode. The matrix size was 64×64 pixels. Using the GMS-5500A/PI (Toshiba Medical Systems), fan beam data were converted to parallel data. In institution O, the SPECT machine has a two-headed $\tilde{\alpha}$-camera (E.CAM; Toshiba Medical Systems) and a LMEGP parallel collimator (Toshiba Medical Systems). The energy range was centered on 158 keV with a width of 20%, and 2-minute data collection per 180° was performed 14 times in continuous mode. The matrix size was 64×64 pixels.

In both facilities, an intravenous injection of two bottles of IMP (167 MBq each) was performed at an interval of 30 minutes, using a constant-rate infusion pump (TE-311; Termo, Tokyo, Japan) for 1 minute (Figure 1). Single photon emission computed tomography data collection was started at the same time as the intravenous injection. Dynamic SPECT scanning was performed for 28 minutes with one rotation of 2 minutes performed two times. The first scan lasted from 0 to 28 minutes and the second scan from 30 to 58 minutes, with each scan collecting data for seven frames of four minutes each. At 20 minutes after the first IMP intravenous injection, acetazolamide (Diamox) loading (17 mg/kg) was performed. At 10 minutes after the first IMP intravenous injection, 4 mL of arterial blood was obtained from the radial artery and the standard input function was calibrated. Whole blood radioactivity was measured with a well counter calibrated to the SPECT apparatus. The calibration between the well counter and the SPECT apparatus was performed using a pool phantom with a uniform diameter of 16 cm filled with ~20 MBq of the ^{123}I solution (height; 15 cm), with SPECT scanning using the same protocol as that for clinical testing. The radioactivity of the sampled solution was measured with the well counter used to measure arterial blood radioactivity in clinical testing. For the first and second scans, all frames were summed and images were reconstructed as described below. Gas measurements in the arterial blood were also performed.

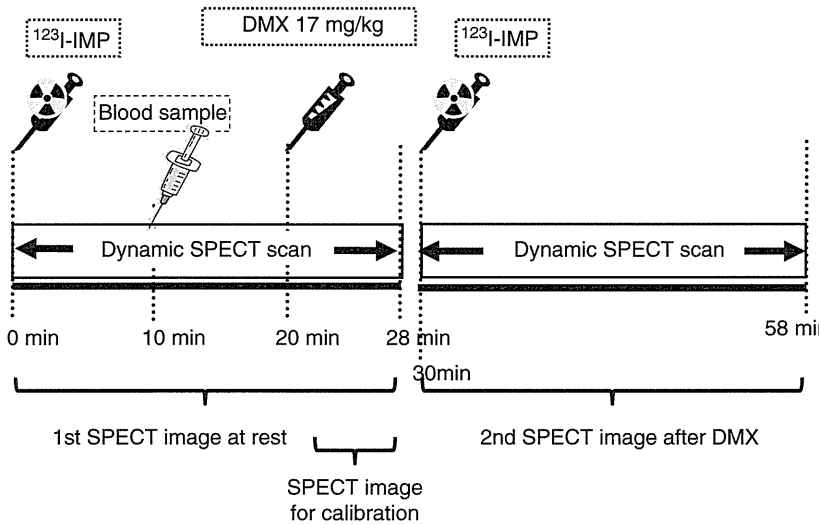

Figure 1 Protocol of the quantitative single photon emission computed tomography/dual-table autoradiographic (QSPECT/DTARG) method. Iodoamphetamine (IMP) was initially intravenously administered for 1 minute and dynamic cerebral blood flow (CBF) SPECT was started simultaneously and continued for 58 minutes (2 minutes × 14 revolutions, two cycles). Ten minutes after IMP administration, arterial blood sampling was performed and an input function was obtained. After 20 minutes, acetazolamide (Diamox) (17 mg/kg) was intravenously administered for 1 minute. After 30 minutes, the same quantity of IMP as in the first administration was intravenously administered for 1 minute. CBF at rest was measured using data collected from 0 to 28 minutes. CBF after acetazolamide challenge was determined using data from 30 to 58 minutes.

Single Photon Emission Computed Tomography Image Reconstruction

Using data from both facilities, images were reconstructed and CBF quantitation was performed using the QSPECT image reconstruction package developed by Iida *et al* (2010) and Kim *et al* (2006). The objectives of QSPECT are to exclude variable factors that occur in SPECT imaging and image reconstruction, to minimize errors between facilities, and to improve quantitation of images. In this software, a series of programs for reconstruction and quantitation are consolidated. Quantitative SPECT extracts head outlines from projection data, makes μ maps, and performs correction of scatted radiation using transmission-dependent convolution subtraction. Transmission-dependent convolution subtraction uses the line spread function obtained from experiments to determine a relational expression among scattered radiation and absorption attenuation coefficient distribution, and the scattered radiation is corrected using this expression. By utilizing the μ map, attenuation correction with ordered subset expectation maximization is performed, the images are reconstructed, and quantitative images are made. These images show the distribution of radioactive concentrations as absolute values expressed as Bq per unit volume.

Single Photon Emission Computed Tomography Image Processing

Single photon emission computed tomography image processing was achieved with the SEE-JET (stereotactic extraction estimation based on the JET study) program (Mizumura *et al*, 2004), using quantitative image data obtained from the QSPECT/DTARG method at rest and after acetazolamide challenge with three-dimensional stereotactic surface projection (3D-SSP). In 3D-SSP, the image tilt of individual subjects is adjusted and linearly converted into 3D stereotaxic coordinates (Talairach standard brain) through the AC–PC line. After anatomic standardization, brain surface extraction is performed with the maximum pixel value shown in the vertical direction in the cerebral cortex from a prescribed brain surface on the stereotaxic coordinate system in the cortex of a standard brain (Minoshima *et al*, 1994). The SEE-JET program can also measure CBF values at rest and after acetazolamide challenge for the territories of the anterior cerebral artery, MCA, and posterior cerebral artery.

The SEE-JET can also automatically calculate the percentage vascular reserve (%VR) for all cerebral coordinate systems, and make 'vascular reserve images'. %VR is defined as ([CBF after acetazolamide challenge−CBF at rest]/CBF at rest) × 100. The program can also classify the severity of hemodynamic brain ischemia for all cerebral coordinate systems into stage 0 to II based on %VR, as described by Nakagawara (1999) and Nakagawara *et al* (2000), and make cerebral surface 'stage images' in 3D-SSP format. The stages are defined as follows: stage 0, resting CBF >15 mL per minute per 100 g and VR >30%; stage I, 34 mL per minute per l00 g (80% of normal CBF) > resting CBF >15 mL per minute per l00 g and 30% > VR >10%, or CBF >34 mL per minute per l00 g and 30% > VR >−30%; and stage II, 34 mL per minute per l00 g > resting CBF >15 mL per minute per l00 g and 10% > VR >−30% (Nakagawara, 1999; Nakagawara *et al*, 2000). Therefore, SEE-JET can perform objective, universal CBF assessment

with automatic analysis that is independent of the operator. The SEE-JET was used on a Windows PC.

Data Analysis

In this study, we investigated CBF in the MCA territories by automatic calculation with SEE-JET. First, Wilcoxon signed-ranks tests were performed on three sets of data for the right and left MCA regions of each patient in institutions O and Y: (1) at rest, (2) after acetazolamide challenge, (3) %VR. Scatter diagrams and linear regression lines were calculated for each data set using Spearman correlation analysis to examine correlations between the two facilities. We also examined interobserver reliability for (1) to (3) using ICCs (intraclass correlation coefficients). Finally, the consistency of MCA CBF measured at the two facilities for each data set was evaluated using Bland–Altman plots (Bland and Altman, 1986). Differences in CBF and %VR were calculated as the value at institution O—that at institution Y. A difference with $P<0.05$ was considered significant.

Results

The subjects were five male and four female patients (59 to 78 years old, mean ± s.d. 68.8 ± 7.1 years old). Five of the patients had ischemic heart disease and one had chronic obstructive pulmonary disease. Four patients were current smokers. Cerebral blood flow in the MCA in each patient in the affected and left hemispheres extracted with SEE-JET, CBF after acetazolamide challenge, and %VR, %Stage II values in the right and left hemispheres are shown in Table 1. These data obtained at the two facilities were compared using Wilcoxon signed-ranks tests. This comparison gave values of $P=0.34$ at rest and $P=0.48$ after acetazolamide challenge for CBF in the right MCA territories ($n=9$); $P=0.91$ at rest and $P=0.64$ after acetazolamide challenge for CBF in the left MCA ($n=9$); $P=0.93$ at rest and $P=0.93$ after acetazolamide challenge for CBF in the right and left MCA ($n=18$); $P=0.24$ for %VR in the right MCA territories ($n=9$) and $P=0.16$ for %VR in the left MCA territories ($n=9$). Therefore, the absolute CBF values and %VR for each patient showed no significant differences between the two facilities.

In Figure 2, three-dimensional cerebral surface CBF extracted images automatically displayed by SEE-JET are shown for data collected in both facilities for patient 3. This patient had symptoms of right internal carotid artery occlusion and the least CVR in the hemisphere among the nine patients. Images from this patient are shown as a representative case. Right and left hemisphere cortical images from both institutions are shown for CBF at rest, CBF after acetazolamide challenge, cerebrovascular reserve, and severity of hemodynamic cerebral ischemia. None of these images showed a major difference between the two facilities, even in a case in which almost all of the right hemisphere was without

?Table 1 Patient characteristics, MCA CBF quantitation, and %stage II values using the SEE-JET program

			Present disease			*Institution O*						*Institution Y*					
						Type of scanner: two-head, parallel-beam collimator						Type of scanner: three-head, fan-beam collimator					
						CBF at rest		CBF after ACZ		%VR[a]		%Stage II[b]	CBF at rest		CBF after ACZ		%VR[a]		%Stage II[b]	
Case	*Age*	*Gender*	IHD	COPD	Smoking	Rt. MCA	Lt. MCA	Rt. MCA	Lt. MCA	Rt. MCA	Lt. MCA	Rt. MCA	Lt. MCA	Rt. MCA	Lt. MCA	Rt. MCA	Lt. MCA	Rt. MCA	Lt. MCA
1	74	F	Yes	Yes	—	43.8	42.4	74.7	71.0	70.7	67.2	0.0	0.0	40.2	39.9	63.4	58.6	57.9	47.1	0.0	0.0
2	78	M	Yes	—	Yes	27.6	25.7	45.5	34.3	64.8	33.2	0.0	3.1	29.3	27.7	42.6	35.5	45.6	28.0	0.0	7.1
3	74	F	—	—	—	28.8	35.2	24.8	52.8	−13.9	50.2	83.6	0.0	30.2	33.5	28.4	54.3	−5.9	61.9	69.1	0.0
4	59	F	—	—	Yes	28.9	29.0	49.6	50.5	71.8	74.2	0.0	0.0	31.9	31.6	50.8	50.5	59.3	59.6	0.10	0.0
5	79	M	—	—	—	32.3	35.2	39.7	49.7	22.9	41.1	4.8	0.10	29.3	31.5	31.7	40.5	8.3	28.4	55.1	7.5
6	62	M	Yes	—	Yes	17.7	22.0	20.6	37.6	16.0	71.2	37.6	0.0	24.9	30.7	24.9	42.1	0.08	37.3	71.0	1.7
7	62	F	—	—	Yes	47.7	76.8	64.0	59.7	34.2	−22.3	0.0	0.0	60.0	58.0	65.1	60.9	8.6	5.00	0.0	0.0
8	76	M	Yes	—	—	37.0	31.3	49.6	49.8	34.2	59.3	0.0	0.0	31.5	28.9	33.1	32.0	4.8	10.9	40.2	38.8
9	74	M	Yes	—	—	25.4	23.5	29.8	24.6	17.5	4.7	22.4	67.0	27.7	26.1	32.9	24.0	19.0	−8.2	25.6	69.9

ACZ, acetazolamide; CBF, cerebral blood flow (mL per 100 g per minute); COPD, chronic obstructive pulmonary disease; IHD, ischemic heart disease; MCA, middle cerebral artery; SEE-JET, stereotactic extraction estimation based on the JET study; VR, vascular reserve.

[a]%VR is defined as ([CBF after ACZ−CBF at rest]/CBF at rest) × 100.

[b]Stage II is classified as severe hemodynamic brain ischemia. The %stage II value is the proportion of the Stage II area in the MCA territory.

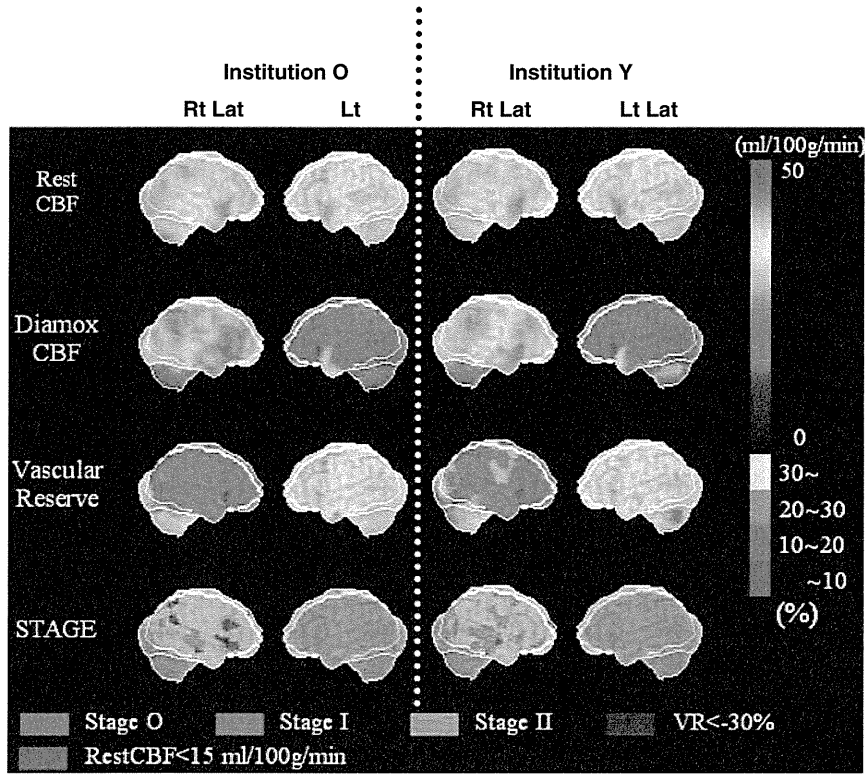

Figure 2 Stereotactic extraction estimation based on the JET study (SEE-JET) images of patient 3 obtained in institutions O and Y. Rt Lat and Lt Lat indicate right hemisphere and left hemisphere outer lateral images, respectively. Cerebral blood flow at rest (Rest CBF), CBF after acetazolamide challenge (Diamox CBF), cerebrovascular reserve (vascular reserve), and severity of hemodynamic cerebral ischemia (STAGE) are shown as three-dimensional cerebral surface images. Images in institutions O and Y are visually almost identical.

cerebrovascular reserve; that is, almost all of the hemisphere had hemodynamic brain ischemia.

In Figure 3, scatter diagrams and linear regression lines comparing data between institutions are shown for MCA CBF in the affected and unaffected hemispheres at rest (Figure 3A), after acetazolamide challenge (Figure 3B), and for %VR (Figure 3C). In Spearman correlation analysis, all four comparisons showed significant correlations between the two facilities (at rest, $r=0.83$, $P<0.01$, $n=18$; after acetazolamide challenge, $r=0.86$, $P<0.01$, $n=18$; %VR, $r=0.82$, $P<0.01$, $n=18$). Regarding interobserver reliability, the ICCs were 0.847 (95% confidence interval (CI): 0.634 to 0.940) for CBF at rest, 0.860 (95% CI: 0.656 to 0.946) after acetazolamide, and 0.727 (95% CI: 0.276 to 0.899) at %VR.

Bland–Altman plots showing the consistency among MCA CBF data measured in the two facilities are shown for MCA CBF at rest (Figure 4A), after acetazolamide challenge (Figure 4B), and for %VR (Figure 4C). For CBF at rest, the mean difference was −0.14 mL per minute per 100 g, the 2 s.d. value was 13.01 mL per minute per 100 g, and 1 of 18 data points was out of the 2 s.d. range. These respective numbers were 3.17 mL per minute per 100 g, 14.39 mL per minute per 100 g, and 1 of 18 data points out of the 2 s.d. range for CBF after acetazolamide challenge; and 12.75%, 34.18% and 2 of 18 data points out of the 2 s.d. range for %VR.

Discussion

Surgical treatment policies for ischemic cerebral diseases have been determined based on the degree of vascular narrowing, as shown in the North American Symptomatic Carotid Endarterectomy Trial study (North American Symptomatic Carotid Endarterectomy Trial Collaborators, 1991). Evaluation of cerebral perfusion has remained at the qualitative level based on relative comparison of the affected and unaffected hemispheres. In recent years, imaging methods such as IMP-ARG (Hatazawa *et al*, 1997; Iida *et al*, 1994, 1996) have been developed and quantitation of CBF has become possible in daily diagnosis. Findings for the relationship between misery perfusion and recurrent symptomatic cerebral infarction suggest that some patients with hemodynamic cerebral ischemia have an increased risk of recurrent ischemic stroke, and that these patients could be detected based on an increase in OEF (Yamauchi *et al*, 1999). Therefore, it is important to evaluate misery perfusion quantitatively to confirm the presence of hemodynamic